CHARACTERISTICS OF SMITH-PURCELL RADIATION FROM DIFFERENT PROFILE GRATINGS*

G. Naumenko[#], B. Kalinin, G. Saruev, NPI, Tomsk, Russia

D. Karlovets, Yu. Popov, A. Potylitsyn, L. Sukhikh, V. Cha, TPU, Tomsk, Russia

Abstract

To choose the most effective grating the absolute coherent SPR characteristics were measured on the 6.2 MeV electron beam. Gratings with lamellar, triangular and so-called "flat" gratings were studied. It was shown the grating consisted of the conductive strips is more preferable target for SPR generation.

INTRODUCTION

Smith-Purcell radiation (SPR) is widely considered as the spontaneous mechanism for FEL (for example[7]). In recent experiments [1,2], the possibility of creating a monochromatic radiation source of the THz range on the basis of the Smith-Purcell radiation (SPR) has been demonstrated. The SPR from low relativistic electrons is also used in orotrons. For the nonrelativistic electron energies ($E_e \leq 100$kev), the approach developed by van den Berg [3,4] ensures a reasonable agreement with experiment [5,6]. In [8] the different models for SPR characteristics calculation were compared for high relativistic electrons. There was shown that the predictions of most models differ by approximately 2 orders of magnitude for the electrons with energy ~20 MeV [9] and by several orders for the electron energies Ee=855 MeV [10]. The available experimental results do not provide an ultimate conclusion on the validity of one of these models.

We distinguish two types of periodic targets, which can be used to generate the SPR: "Volume" gratings (a lamellar grating (Fig. 1) and a grating which consist of a periodic set of conducting strips separated by vacuum gaps) and "Flat" gratings (consisting of separate conducting strips having the thickness essentially smaller than a wavelength).

The coherent Smith-Purcell radiation (CSPR) emitted from the first-type targets with different profile was studied experimentally by several experimental groups ([11, 12]). However, all these works differ in the applied methods. On the other hand, it was shown in works [13, 1] that flat targets are more effective in order to obtain an intensive monochromatic radiation. Therefore, the direct comparison of the measured characteristics of radiation from these targets is difficult. That is why the research of the CSPR characteristics from the targets of different types but under similar conditions is desirable.

MODELS

There are few theoretical models to calculate the SPR characteristics for the different grating profiles. We consider here three models: van den Berg's (vdB) model [3] (applicable for volume gratings), surface current (SC) model [14,15] (the SPR is considered as a radiation generated by the current induced by the field of a particle moving in vacuum close to a perfect conducting periodic surface), and resonant diffraction radiation (RDR) model [16] (for gratings consisting of infinitely thin perfect conducting strips separated by vacuum gaps).

Comparison of models for thin strips grating

We use for calculations the formulas from [8] for the case $\Phi = 0$ (see Fig. 1)
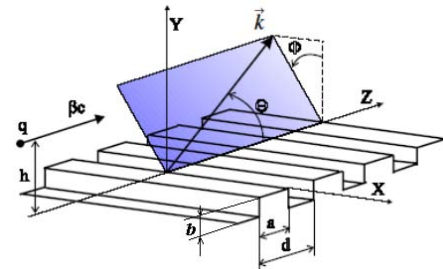

Fig. 1. Scheme of the Smith-Purcell radiation generation

The calculations (Fig. 2) were made for the Lorenz-factor $\gamma = 12$ and the grating period $d = 8$ mm.
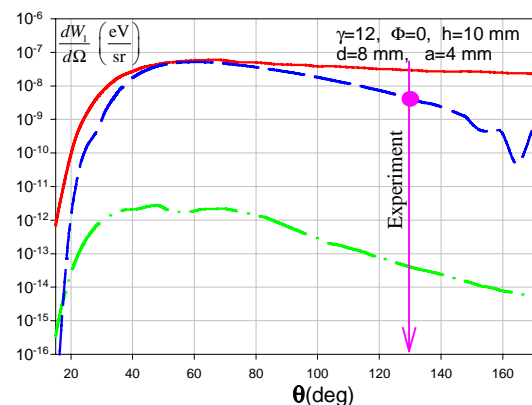

Fig. 2. Angular distribution of the SPR intensity for a flat grating according to the RDR model (red solid line), surface current model (blue a dashed curve) and for van den Berg's model (green dash-dotted line, $b/d = 0.001$).

We can see from the Fig. 2 a large discrepancy between radiation yields obtained using these three models.

SPR from different type structures

Let us compare the angular distribution of the calculated SPR intensity from different gratings according to the van den Berg's model (Fig. 3): for a volume grating with vacuum gaps and strips 4 mm thick and a for flat grating with $b/d = 0.001$. One may see from the Fig.3 that the intensity of the SPR from a "thick" grating is by 2 orders of magnitude greater.
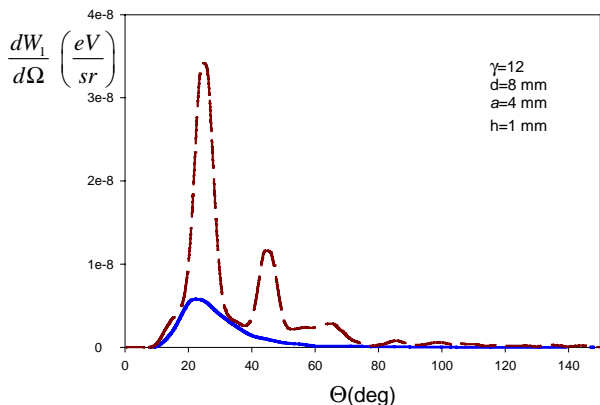

Fig. 3. Angular distribution of the SPR intensity for a flat grating (blue solid line; is multiplied by 10) and for a volume grating (red dashed line).

Coherence

Let's consider the approximation for the case when the size of an electron beam is much smaller than the impact parameter h. In this approximation in terms of the Smith-Purcell geometry longitudinal and transverse distributions of electrons in a bunch are factorized, which enables one to extract the longitudinal and transverse geometric form-factors of a bunch in the form of separate factors. In this case only the longitudinal form-factor plays the essential role (see [17]).

The typical dependence of the longitudinal form-factor via the wavelength for the normal (Gauss) distribution of electrons in a bunch is shown in Fig. 4.
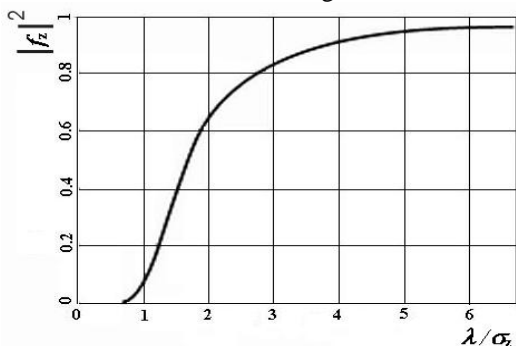

Fig.4 The Dependence of the squared form-factor module on the radiation wavelength for the normal longitudinal distribution of electrons in a bunch with bunch length σ_z.

The registered emission of radiation in the wavelength range $\Delta\lambda$ may be written as:

$$Y(h,\theta,\sigma_z) = N^2 \cdot \int\limits_{\Delta\lambda} \left| f_z\left(\frac{\lambda}{\sigma_z}\right) \right|^2 \cdot \int\limits_{\Omega} \frac{d^2 W_{SP}(\lambda,h,\theta)}{d\lambda d\Omega} d\Omega \cdot \varepsilon(\lambda) d\lambda$$

where $W_{sp}(\lambda,h,\theta)$ is the intensity of incoherent SPR, $\varepsilon(\lambda)$ is the spectral efficiency of a detecting system.

EXPERIMENTAL SETUP AND TECHNIQUE

Electron beam

The experiment was carried out on the extracted electron beam of the microtron of the Tomsk Institute for the Nuclear physics.

The scheme of the the experimental zone setup was changed depending on a problem statement (see Figs 5,6). The beam parameters are given in Table 1.

Table 1:   Electron beam parameters

Electron energy	6.1 MeV
Macro-pulse duration	$\approx$4 ms
Pulse repetition rate	1 – 8 Hz
Micro-pulse length	$\approx$6mm
Number of electrons per micro-pulse	10^8
Number of micro-pulses per macro-pulse	10^4
Beam size at the microtron output	4×2 mm^2
Emittance: horizontal vertical	$3 \cdot 10^{-2}$ mm$\times$rad $1.5 \cdot 10^{-2}$ mm$\times$rad

Detector

To register the radiation within a millimeter wavelength range the authors applied the room-temperature detector operating on the basis of a broadband antenna supplied by a high-frequency diode. The latter was produced at the Institute for Semiconducting Devices (Tomsk, Russia). The main parameters of the detector for room temperature are:

wavelength range: $\Delta\lambda = 3 \sim 20$ mm,
sensitivity = 0.3 V/mWatt

Techniques for angular measurements

Cut-off filters cutting passage of the radiation with the wavelengths, exceeding the critical length λ_c, were used.

To compare our data with the theoretical calculations obtained using the classical models we should be sure that the obtained experimental results correspond to the far zone approximation. In paper [18] it was shown that the effect of pre-wave zone may be suppressed while applying the parabolic optics, when a detector is placed in the focus of a parabolic reflector. For this purpose the parabolic reflector with diameter equal to 140 mm and the focal distance equal to 430 mm was used during the experiment.

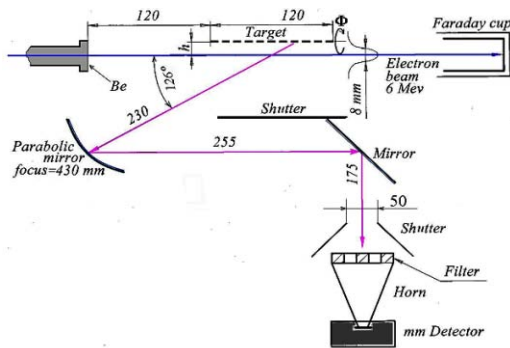The scheme for the azimuth angular dependence measurements is presented in Fig. 5

Fig. 5. Experiment scheme for azimuth dependences measurement

The scheme of the of radiation intensity dependences on the polar angle measurements is shown in Fig. 6. Detector together with the parabolic reflector was fixed on a radial rod, which rotated around the target at the angle θ.
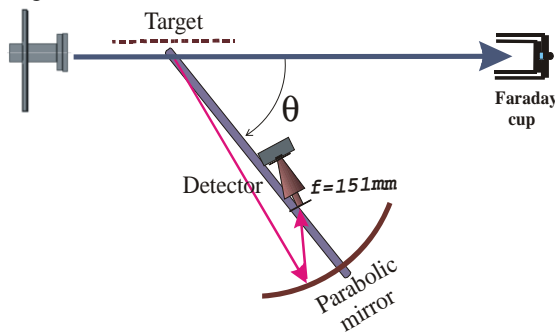

Fig.6. Experimental scheme for the angular dependences measurement

Targets

Table 2. Target parameters (size unit is mm)

In the experiment the characteristics of the radiation from both volume and flat targets were studied. The parameters of the targets used are given in the Table 2.

EXPERIMENTAL RESULTS

The measurements of the azimuth angular intensity distributions of the CSPR were made with the arrangement presented in Fig. 5 when the value of the polar observation angle was equal to $\theta = 130°$, which corresponds to the wavelength of SP radiation $\lambda = 13.2$ mm. Fig. 7 presents the azimuth angular distribution of the CSPR from a flat target 1 with the use of the two cut-off filters having the critical wavelength $\lambda_c=14$ mm and $\lambda_c=17.5$ mm. The value of $\Phi = 0$ corresponds to the direction in the plane which is perpendicular to the target plane. The measurements with the use of cut-off filters with $\lambda_c < 14$ mm give the values which practically coincide with the background.
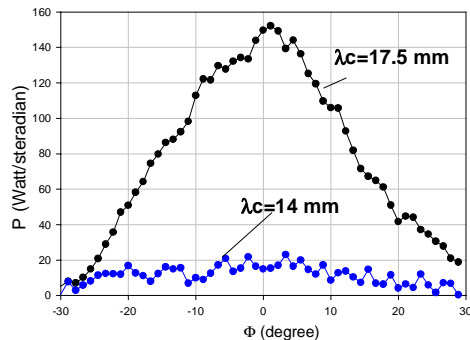

Fig.7. Azimuth CSPR distribution from the target 1 with different cut-off filters.

The absolute azimuth intensity distribution of the CSPR from targets 1, 2, 4 with different profiles for $\lambda_c=17.5$ mm is presented in Fig. 8.
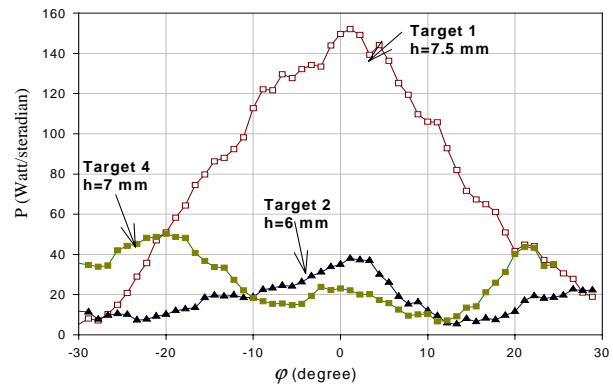

Fig.8. Azimutal CSPR distribution from flat and volume targets for $\lambda_c=17.5$mm.

The azimuth intensity distribution of the CSPR with different values of the impact-parameter (Fig. 9) shows the principle influence of the impact-parameter value.

The measurements of the dependences of the CSPR intensity on the value of the polar observation angle were carried out according to the scheme shown in Fig. 6 with the value of the azimuth angle equal to $\Phi=0$.
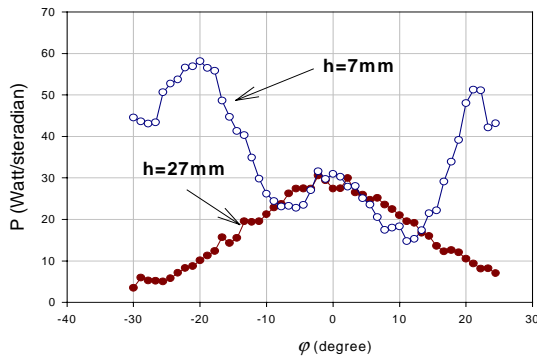
Fig.9. Azimutal CSPR distribution from target 4 for different values of impact-parameter and λc=17.5mm

The radiation cutting off across the wavelength was provided by a cut-off wave-drive with λc=17.5 mm to decrease the background contribution from a RF system of an accelerator. The typical CSPR intensity dependence via the polar observation angle for h=7 mm is shown in Fig. 10.
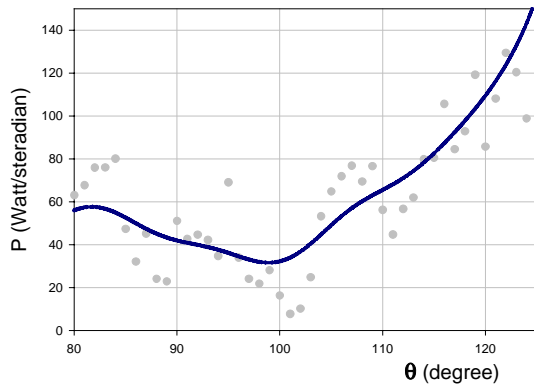

Fig.10. Polar dependence of CSPR from flat target 1

Discussion

Suppression of the pre-wave zone effect by means of wave optics on this experiment enables one to compare the obtained experimental results with the conclusions of the SPR theory in the far zone (Table 3).

Table 3: Target efficiency (experiment)

Target	CSPR density $dW/d\Omega$	
	Watt/sr	eV/sr per electron and per period
1. Flat thin target	0.153	$4.8\cdot10^{-9}$
2. Flat thick target	0.039	$1.2\cdot10^{-9}$
3. Volume target with square profile	0.012	$0.37\cdot10^{-9}$
4. Volume target with triangular profile	0.029	$0.9\cdot10^{-9}$

On the coherency conditions the CSPR is observed in the range of polar angles exceeding $100^{°}$ (see Fig.10). The measured azimuth distribution of the targets having a different profile under similar conditions enables us to

assert as for the maximum efficiency of flat conducting thin-stripped targets (Table 3).

Comparing the absolute experimental data from Table 3 with the theoretical predictions (Fig. 2) ascertain that the RDR and SC models .

REFERENCES

[1] Yukio Shibata, Shigeru Hasebe, et. al., Phys. Rev. E 57, 1061 (1998).
[2] S.E. Korbly, A. S. Kesar, J.R. Sirigiri, and R. J. Temkin, Phys. Rev. Lett. 94, 054803 (2005).
[3] P.M. van den Berg, J. Opt. Soc. Am. 63, 1588 (1973).
[4] P.M. van den Berg, J. Opt. Soc. Am. 63, 689 (1973).
[5] A. Gover, P. Dvorkis, and U. Elisha, J. Opt. Soc. Am. B 1, 723 (1984).
[6] Y.N. Adischev, A.V. Vukolov, D.V. Karlovets, A. P. Potylitsyn, and G. Kube, Pis'ma Zh. Eksp. Teor. Fiz. 82, 192 (2005) [JETP Lett. 82, 174 (2005)].
[7] H. Backe, W. Lauth, H. Mannweiler, et. al., in NATO Workshop ''Advanced Radiation Sources and Applications'' (Springer, New York, 2006), pp. 267-282.
[8] D. V. Karlovets* and A. P. Potylitsyn, Phys. Rev. ST AB 9, 080701 (2006)
[9] A.S. Kesar, Phys. Rev. ST Accel. Beams 8, 072801 (2005).
[10] G. Kube, H. Backe, H. Euteneuer, et.al., Phys. Rev. E 65, 056501 (2002).
[11] D. C Nguyen, Nucl. Instrum. Methods Phys. Res., Sect. A 393, 514 (1997).
[12] S.E. Korbly, W.J. Brown, M.A. Shapiro, and R. J. Temkin, in Proceedings of the Particle Accelerator Conference, 2001, Chicago, USA (IEEE, New York, 2001), pp. 2347-2349.
[13] A. Doria, G. P. Gallerano, E. Giovenale, G. Messina, G. Doucas, M. F. Kimmitt, H.L. Andrews, and J. H. Brownell, Nucl. Instrum. Methods Phys. Res., Sect. A 483, 263 (2002).
[14] J. H. Brownell, J. Walsh, and G. Doucas, Phys. Rev. E 57, 1075 (1998).
[15] J. H. Brownell and G. Doucas, Phys. Rev. ST Accel. Beams 8, 091301 (2005).
[16] A. P. Potylitsyn, Nucl. Instrum. Methods Phys. Res., Sect. B 145, 60 (1998).
[17] A. N. Aleinik, A. S. Aryshev, B. N. Kalinin, G. A. Naumenko et.al, JETP Letters, 76, 6, (2002), p. 337.
[18] B. N. Kalinin, G.A. Naumenko, A.P. Potylitsyn, G.A. Saruev,L. G.Sukhikh, and V.A. Cha, JETP Letters, 84, 3, (2006), p. 110.
[19] J.H. Brownell, J. Walsh, G. Doucas, Phys. Rev. E 57 (1998)1075.
[20] A.P. Potylitsyn, Phys. Lett. A 238 (1998) p.112.